Hugh P. Rice*[1], Michael Fairweather[1], Jeffrey Peakall[2], Timothy N. Hunter[1], Bashar Mahmoud[1], and Simon R. Biggs[a1]

[1] School of Process, Environmental and Materials Engineering

[2] School of Earth and Environment

University of Leeds, Leeds LS2 9JT, United Kingdom

* Correspondence to h.p.rice@leeds.ac.uk

Measurement of particle concentration in horizontal, multiphase pipe flow using acoustic methods: limiting concentration and the effect of attenuation

Abstract

An acoustic dual-frequency concentration inversion method, in which the backscattered acoustic signal received by transducers operating in the megahertz range is used to determine the concentration profile in suspensions of solid particles in a carrier fluid and which was originally developed for environmental applications, is applied to arbitrary suspensions of general engineering interest. Two spherical glass and two non-spherical plastic particle types with a range of size distributions and densities are used. Particle concentration profiles in horizontal turbulent pipe flow at Reynolds numbers of 25 000 and 50 000 – below and above the critical deposition velocity, respectively - and nominal concentrations of 0.5, 1 and 3 % by volume are presented for the four particle species, using measured backscattering and attenuation coefficients. In particular, the effects of particle size, density and flow rate on the transport and settling behaviour of suspensions are elucidated. The results demonstrate the potential of this method for measuring the degree of segregation in real suspensions and slurries across a range of challenging application areas, such as the nuclear and minerals processing industries. The limitations of the method are explored in detail through an analysis of the acoustic penetration depth and the application-specific maximum measurable concentration, both of which can be used to determine the most appropriate acoustic frequencies and measurement

[a] Current address: Faculty of Engineering, Architecture and Information Technology, University of Queensland, Brisbane, QLD 4072, Australia

configuration in a particular case.

Highlights

- Marine model for measuring suspended solid fraction adapted for general use.
- Glass and plastic particles tested at several fractions in horizontal pipe flow.
- Clear differences observed between species and settling and non-settling flows.
- Limiting concentration and penetration depth derived to inform future experiments.
- Method has potential for use in several engineering applications.

Keywords: acoustic backscatter; sediment transport; scattering; attenuation; instrumentation.

1 Introduction

The flow of solid-liquid suspensions in pipes has generally been categorised as follows: Non-settling, in which the solid fraction remains fully suspended in the carrier fluid; unhindered-settling, in which suspended particles can freely settle under gravity; or hindered-settling, in which hindrance to downward-moving particles is provided by upward-moving carrier fluid, through the conservation of mass (Crowe, 2006; Doron and Barnea, 1995; Wasp *et al.*, 1977). Alternatively, five flow regimes for suspensions, and various combinations thereof, are commonly described as follows: homogeneous (or pseudo-homogeneous), in which all particles are suspended and the concentration and velocity is uniform across the diameter of the channel; heterogeneous, in which a concentration gradient exists in the suspension; flow with a moving bed, or sometimes "saltation" flow, in which some fraction of the suspended particles has settled and formed a sediment bed that moves along the channel; flow with a stationary bed, in which at least part of the sediment is stationary relative to the channel; or plug flow, in which the solids span the diameter of the channel and move *en masse* (Crowe, 2006).

Most commonly, the five flow regimes described above are delineated by the transition velocities U_{c1} to U_{c4}, respectively (Crowe, 2006). Of these, U_{c1} represents the velocity above which all solids are suspended homogeneously, while U_{c2} (or U_c) is the velocity above which solids begin to settle out of a heterogeneous suspension and form a sediment bed. Some confusion exists because the term "critical velocity" (U_{min}) has also been used to describe the velocity at which the pressure drop reaches a minimum (Doron and Barnea,

1993; Doron *et al.*, 1987). However, such confusion is avoided in this study, with U_c being referred to as the critical deposition velocity (Oroskar and Turian, 1980; Soepyan *et al.*, 2014), although they have been given several other names in the literature ("critical velocity", "minimum transport velocity" or "deposition velocity": Crowe, 2006; Harbottle *et al.*, 2011).

In this study, the influence of particle size and concentration on the flow pattern – specifically the local concentration profile with respect to vertical position – above and below the critical deposition velocity is investigated. There follows a summary of some models and experimental studies of concentration profiles in heterogeneous suspensions in pipes and channels, which are also listed in Table 1, in which ϕ is the particle volume fraction (which is used alongside the mass concentration, M, hereafter), d is the particle diameter, and the Reynolds number, Re, is defined as follows:

$$\mathrm{Re} = \frac{U_b D}{\nu}, \qquad [1]$$

where U_b is the bulk (average) axial flow velocity, D is the pipe diameter or channel width and ν is the kinematic viscosity of the carrier fluid.

Table 1: Multiphase and high-concentration pipe and channel flow studies.

Reference	Method	D (mm)	Re (10^3)	Particle properties
Shook *et al.* (1968)	Gamma rays	24.7 × 101 (channel)	Not applicable	Sand, d = 153-510 μm, ϕ = 2.5-28 %; nickel, d = 135 μm, ϕ = 2.4-15 %
Karabelas (1977)	Sampling, modelling	50.4 and 75.3	≈ 3-55	Resin, d = 210 and 290 μm, ρ = 1126 kg m^{-3}, ϕ ≈ 3-6.5 %
Zisselmar and Molerus (1979)	LDA	50	≈ 50	Glass, d = 53 μm, ρ = 2510 kg m^{-3}, ϕ ≤ 5.6 %
Tsuji and Morikawa (1982)	LDV, Pitot probe	30.5	11.7-38.9	Plastic, d = 0.2 and 3.4 mm, ρ = 1000 kg m^{-3}, ϕ ≤ 6 %; KCl tracers, d = 0.62 μm
Gillies and Shook (1994)	Gamma rays	53.2-495	95.8-1,880	Sand, d = 0.18-2.4 mm, ρ = 2650 kg m^{-3}, ϕ = 6-45 %
Pugh and Wilson (1999)	Gamma rays	105	87.2-193	Sand, d = 1.05 mm, ρ = 1530 kg m^{-3}, ϕ = 3.6-10.5 %; Bakelite, d = 0.30 and 0.56 mm, ρ = 2650 kg m^{-3}, ϕ = 1.2-5.5 %
Admiraal and García (2000)	Acoustic probe	300 × 100 (channel)	Not applicable	Sand, d = 120 and 580 μm
Kaushal *et al.*	Modelling	55, 105	Large	Zinc, iron and copper tailings

Table 1: Multiphase and high-concentration pipe and channel flow studies.				
Reference	Method	D (mm)	Re (10^3)	Particle properties
(2002)			range	(comparison with several studies)
Gillies *et al.* (2004)	Resistivity probe	103	134-309	Sand, d_{50} = 90 and 270 μm, ϕ = 10-45 %
Ekambara *et al.* (2009)	Numerical	50-500	Large range	All sand or sand-like, d = 90-500 μm, ϕ = 8-45 %
Matoušek (2009)	Gamma rays	150	66-311	Sand, d = 370 μm, ρ = 2650 kg m^{-3}, ϕ = 3.1-34.9 %
Furlan *et al.* (2012)	Acoustic probe	25.4	50.8-88.9	Glass, d = 195 μm, ρ = 2500 kg m^{-3}, ϕ = 7 and 9 %
Capecelatro and Desjardins (2013)	Modelling	51.5	46.7 and 85	Sand-like, d = 165 μm, ρ = 2650 kg m^{-3}, ϕ = 8.4 %
Kaushal and Tomita (2013)	Modelling	Several	Several	Glass and sand (comparison with several studies)
Legend: d and d_{50} are particle diameter and 50th percentile of size distribution; ϕ is volume fraction occupied by particles; Re is Reynolds number.				

Karabelas (1977) derived a model for vertical particle concentration in pipes and channels and found excellent agreement with his own experimental results (plastic spheres in kerosene, oil, and mixtures thereof) and those of Durand (1952) (sand in water). The "two-layer" model of Gillies *et al.* (1991), which was tested against experiments, incorporates a layer of suspended "fines", *i.e.* buoyant particles, and carrier fluid, and a bed with two components, a "contact load" which dissipates energy through friction with the wall, and a "suspended load", whose weight is held by the carrier fluid. The model has been verified very successfully against experimental concentration profile data for coarse sand suspensions by Gillies and Shook (1994), and has undergone a number of refinements, including extension to higher volume fractions around the deposition velocity (ϕ > 35% or so) (Gillies *et al.*, 2000) and higher velocities (Gillies *et al.*, 2004).

Pugh and Wilson (1999) found the particle concentration varies linearly with height above stationary beds. Admiraal and García (2000) measured the particle concentration above a sand bed in a water channel using a single-frequency acoustic method (at f = 2.25 MHz) in which the mean-squared voltage received by the transducer was correlated with the suspended solids concentration. Gillies *et al.* (2004) presented concentration profiles for sand in pipe flow (with water); it is interesting to note that group's "two-layer" or "SRC" (Saskatchewan Research Council) model (Gillies and Shook, 2000) very accurately predicted the mean delivered solids concentration in high-concentration suspensions (up

to several tens of percent by volume).

The simulations and experimental results of Ekambara *et al.* (2009) closely matched each other and numerical data from the literature in terms of concentration, velocity and pressure drop. In one of several related papers, Matoušek (2009) presented concentration profiles above a partially stationary sand bed and modelled the solid fraction as being composed of three layers – a stationary bed, a shear layer and a fully suspended layer – in contrast to the two-layer model of Gillies *et al.* (1991; 2004). Using an acoustic power-spectrum measurement method (centred on f = 2.25 MHz), Furlan *et al*. (2012) also found good agreement between experimental and numerical results in horizontal and vertical pipe flow with glass beads in water.

In the fully coupled numerical simulations of Capecelatro and Desjardins (2013), Lagrangian tracking was used to follow the motion of individual solid particles. Excellent agreement was found between the predictions of the simulation and an experimental dataset taken from the literature (Roco and Shook, 1985). Kaushal and Tomita (2013) modified an earlier model (Kaushal and Tomita, 2002a) and found excellent agreement with several earlier experimental studies (Gillies and Shook, 1994; Kaushal *et al.*, 2005; Matoušek, 2009).

There are several objectives in this paper. The first is to investigate flows at lower concentrations, specifically of the order of a few percent by volume, which are of particular interest, both in terms of fluid mechanics and the wide range of industrial applications. Such flows occupy the transition between dilute and concentrated flows, at which fluid-particle and inter-particle interactions – both collisional and hydrodynamic – begin to significantly influence the flow characteristics. Despite the industrial relevance of such flows, there is a scarcity of available data at low concentrations, although some exist at higher concentrations (Ekambara *et al.*, 2009; Gillies *et al.*, 2004; Karabelas, 1977; Kaushal and Tomita, 2002b) and in flows with a stationary bed component (Matoušek, 2009; Pugh and Wilson, 1999).

Second, a measurement system was sought that is not subject to the shortcomings of those described earlier and has as many of the following properties as possible:

- Can be applied to flows of general engineering interest;
- Has suitably high temporal and spatial resolution;
- Is preferably able to gather data profiles rather than time-consuming, point-wise

data;

- Is affordable;
- Is simple to deploy;
- Can be used without intruding into the flows;
- Is not computationally demanding, such that post-processing can be done *in situ*;
- Is as safe as possible, preferably employing non-ionizing radiation.

The ultrasonic system used in this study satisfies all these criteria for the purpose of the application. The third objective is to assess the suitability to general engineering applications of a model relating the acoustic backscatter signal received by an active emitter-receiver transducer to the physical and acoustic properties of suspended solid particles (Thorne and Hanes, 2002). The backscattering and attenuation coefficients that are required for implementation of the model have been measured previously only for quartz sand-type particles, *i.e.* marine/coastal sediment (Thorne and Meral, 2008). The model was therefore modified in a preceding paper (Rice *et al.*, 2014) to be applicable to suspensions of particles with arbitrary properties of engineering interest. Values of the backscattering and attenuation coefficients for four particle types (two spherical glass, two non-spherical plastic), and a novel method for measuring them, were presented. With these measured coefficients, some concentration profiles in horizontal pipe flow were computed for validation purposes using an existing explicit, dual-frequency concentration inversion method (Hurther *et al.*, 2011). In the present study, a wider range of normalised concentration profiles, arranged by particle type and Reynolds number, is presented.

A number of concentration inversion methods exist (Hanes, 2012; Hanes *et al.*, 1988; Lee and Hanes, 1995; Thorne and Hardcastle, 1997; Thosteson and Hanes, 1998) many of which were reviewed in detail by Thorne and Hanes (2002) and Thorne *et al.* (2011). The issue of numerical instability is an important and well known one in both implicit and explicit inversion methods, as it can cause computed particle concentrations to deviate very significantly from the true values to an extent that increases with distance from the transducer(s). More specifically, such deviations are caused by the accumulation of uncertainties with distance, as the computation of particle concentration at a particular measurement point relies on the values computed at preceding points in the majority of inversion methods. Uncertainties exist in the particle size distribution and the resulting acoustic attenuation and scattering properties thereof, temperature variations contribute to errors in the acoustic properties of both the solid and fluid phases, and non-linear statistical effects may also be significant (Hay, 1991).

This kind of numerical instability was present in both the acoustic methods described above, namely those of Furlan *et al.* (2012) and Admiraal and García (2000). In the latter case, an approximation at low concentrations (up to ϕ = 1 % or so) was made that avoided the requirement for a correction for attenuation. However, this approach is not ideal in general and an inversion method was sought for the present study that has the potential for general applicability – *i.e.* in a range of flow geometries and particle concentrations not limited to ϕ < 1 %. The model described by Hurther *et al.* (2011) was chosen for the present study because it is not subject to numerical instabilities – as the concentration is computed at each measurement point independently – and has subsequently been found to perform significantly better than several other acoustic inversion methods in the far field (Thorne *et al.*, 2011).

The structure of this paper is as follows. The Thorne and Hanes (2002) and Hurther *et al.* (2011) models are briefly reiterated in Section 2. The pipe flow loop and the method of operation of the *UVP-DUO* instrument are described, and the physical properties of the particle species are summarised in Section 3. An investigation of the limitations of the method *via* the acoustic penetration depth and the limiting concentration – *i.e.* the maximum measurable concentration as dictated by the desired maximum measurement distance – is presented in Section 4.1. Some example cases are given to demonstrate how the penetration depth and limiting concentration can be used to select the most appropriate acoustic frequency and measurement domain for any specific application. A full set of concentration profiles, at four nominal particle volume fractions and two flow rates – Re ≈ 25 000 and 50 000, *i.e.* below and above the critical deposition velocity, respectively – are presented in Section 4.2. Lastly, the absolute and relative error due to uncertainties in the acoustic attenuation coefficient, ξ_h, is illustrated for one run as an example in Section 4.3, with the corresponding error analysis given in the appendix; the error in the attenuation due to water as a result of temperature variations is also quantified and the conditions under which this error becomes comparable to the attenuation due to suspended particles is investigated in detail.

2 Concentration inversion methods in suspensions of solid particles

Of the studies listed in Table 1 and described in Section 1, only those of Admiraal and García (2000) and Furlan *et al.* (2012) employed acoustic methods to measure the particle concentration profile. Although distinct, the methods are similar in that they employ the scattering and attenuation properties of the suspension, rather than other properties, such

as speed of sound, compressibility or acoustic impedance (Challis *et al.*, 2005; McClements, 1991; Povey, 1997).

In this section, one specific acoustic model based on backscattering and attenuation – that of Thorne and Hanes (2002) and Hurther *et al.* (2011) – is outlined, since it is used as the basis of this study, and the reader is referred to a related paper (Rice *et al.*, 2014) for a more thorough description. The received root-mean-square (RMS) voltage, V, excited in the ultrasonic transducers by backscattered energy is related to the mass concentration of suspended particles, M, and varies with distance from the transducer, r, as follows (Thorne and Hanes, 2002):

$$V = \frac{k_s k_t}{\psi r} M^{1/2} e^{-2r\alpha}, \quad [2]$$

where α is the total attenuation due to scattering and absorption, such that

$$\alpha = \alpha_w + \alpha_s, \quad [3]$$

where α_w and α_s are the attenuation due to water and solid particles, respectively; k_s is the sediment backscatter constant and incorporates the backscattering properties of the particles; and k_t is a system constant. Here, as in a related paper (Rice *et al.*, 2014), k_s and k_t are expressed as the combined backscattering and system coefficient, K, such that

$$K = k_s k_t. \quad [4]$$

The mass concentration, M, is used interchangeably in this study with the volume fraction, ϕ, which are related as follows:

$$\phi = \frac{M}{\rho_s}, \quad [5]$$

where ρ_s is the density of suspended particles. The near-field correction factor, ψ (Downing *et al.*, 1995) tends to unity in the far field, *i.e.* when $r \gg r_n$, where r_n is the near-field distance given by

$$r_n = \pi a_t^2 / \lambda \quad [6]$$

a_t is the radius of the active face of the transducer and λ is the ultrasound wavelength. The attenuation due to water, α_w, is calculated according to the expression given by Ainslie and McColm (1998), and the attenuation due to solid particles, α_s, is found by integration in the general case, in which both M and the particle attenuation coefficient, ξ, vary with distance from the transducer, as follows:

$$\alpha_s = \frac{1}{r}\int_0^r \xi(r\,)\, M(r\,)\mathrm{d}r\,. \qquad [7]$$

The coefficients K and ξ, then, incorporate the backscattering and attenuation properties of the suspended solid particles, but published data only exist for quartz sand (Thorne and Meral, 2008). In a related paper (Rice *et al.*, 2014) a novel method for measuring K and ξ for arbitrary materials was described, and measured values of K and ξ for spherical glass and non-spherical plastic particle species are summarised in Table 2. A short description of the method follows. First, Equation [7] is simplified for the case of a homogeneous suspension, *i.e.* one in which neither M nor the particle size distribution (and therefore ξ) vary with distance, such that

$$\alpha_{sh} = \xi_h M, \qquad [8]$$

where the h subscript denotes the case of homogeneity. Next, the range-corrected echo amplitude, G, is defined as follows:

$$G = \ln(\psi r V). \qquad [9]$$

By rearranging Equation [2] then taking the second derivative with respect to r and M, the following expression for the attenuation coefficient in homogeneous conditions, ξ_h, is obtained:

$$\xi_h = -\frac{1}{2}\frac{\partial}{\partial M}\left[\frac{\partial}{\partial r}[\ln(\psi r V)]\right] = -\frac{1}{2}\frac{\partial^2 G}{\partial M\,\partial \mathrm{r}}. \qquad [10]$$

The backscatter and system coefficient, K_h, is then calculated by rearranging Equation [2] for K_h (noting the identity in Equation [4]) and evaluating it using the measured value of ξ_h, then averaging over distance, r, and the suspended concentration, M. So, the method relies on measuring ξ_h *via* the second derivative of the range-corrected echo amplitude, G, with respect to r and M. In practice, then, this requires that the calibration suspensions be of

known, homogeneous concentrations. It is to this homogeneity that the subscript h in ξ_h and K_h refer, and not to the suspensions in which the coefficients can thence be used, which can have arbitrary concentration profiles, as described below.

The purpose of any concentration inversion method is to express the mass concentration of particles, M, in terms of the received RMS voltage, V, and other known quantities – including K and ξ – by rearrangement of Equation [2], but it is clear from Equations [2], [3] and [7] that such inversions are difficult because M appears more than once, and many such implicit and explicit inversion methods suffer from numerical instability in the far field (Thorne and Hanes, 2002), as described in the preceding section. However, one explicit dual-frequency inversion method (Hurther *et al.*, 2011; Thorne *et al.*, 2011) avoids such instabilities and the particle concentration can be calculated at any position from the transducer independently. According to this method, the particle mass concentration is obtained by algebraic manipulation of Equation [2] as follows:

$$M = J_1^{(1-\xi_1/\xi_2)^{-1}} J_2^{(1-\xi_2/\xi_1)^{-1}}, \qquad [11]$$

where J is as defined below and the subscripts 1 and 2 relate to each ultrasonic frequency at which RMS voltage profiles must be recorded.

$$J(r) \equiv Me^{-4\int_0^r \xi(r)M(r)\mathrm{d}r} = V^2(r)/\Phi^2(r), \qquad [12]$$

where V is the recorded RMS voltage and Φ^2 contains the known variables and coefficients and is as follows:

$$\Phi^2 \equiv \left(\frac{K}{\psi r}\right)^2 e^{-4r\alpha_w}. \qquad [13]$$

3 Materials and methods

Four particle species were used, the physical and acoustic properties of which are summarised in Table 2, and were chosen because they represented a range of sizes, densities and shapes, and therefore a range of backscattering and attenuation properties. A full description of the methods and apparatus used to determine those properties are given in the preceding paper (Rice *et al.*, 2014) and were summarised in Section 2. The dual-frequency method described in Section 2 requires that the ratio ξ_1/ξ_2, as it appears in

Equation [11], be "sufficiently different from unity" (Hurther *et al.*, 2011). It is clear from the values of ξ given in Table 2 that this condition was, indeed, satisfied for all four particle species.

Table 2: Physical and acoustic properties of particle species. All species supplied by Guyson International, Ltd. All data from Rice *et al.* (2014).

Particle species	Small glass (Honite 22)	Large glass (Honite 16)	Small plastic (Guyblast 40/60)	Large plastic (Guyblast 30/40)
Shape	Spherical	Spherical	Non-spherical	Non-spherical
d_{10} (μm)	26.8	53.5	269	459
d_{50} (μm)	41.0	77.0	468	691
d_{90} (μm)	56.6	104	712	966
ρ (10^3 kg m^{-3})	2.45	2.46	1.54	1.52
ka (2 MHz)	0.174	0.327	1.99	2.93
ka (4 MHz)	0.348	0.654	3.97	5.87
K_1 (2 MHz)	0.00229	0.00363	0.0100	0.0163
K_2 (4 MHz)	0.00430	0.00699	0.0239	0.0182
ξ_1 (2 MHz)	0.0182	0.0212	0.627	1.34
ξ_2 (4 MHz)	0.0694	0.135	2.74	2.73

Legend: d_{50} is median particle size; ρ is density; k is ultrasonic wavenumber; a is particle radius (*i.e.* $d_{50}/2$); K is backscattering and system constant; ξ is attenuation coefficient; subscripts 1 and 2 refer to ultrasonic frequency f = 2 and 4 MHz, respectively.

Based on a number of criteria that were described earlier (cost, portability and ability to operate remotely, ease of operation and computational requirements), an ultrasonic system was chosen for the present study, consisting of a *UVP-DUO* signal processor (*Met-Flow*, Switzerland) and two transducers operating at 2 and 4 MHz. Two pencil-type piezoelectric ultrasonic transducers (*Imasonic*, France) were mounted on a horizontal test section of a recirculating pipe flow loop (Figure 1) with an inner diameter of D = 42.6 mm.. They were inserted through holes in the upper wall of the pipe and were in contact with the suspensions.

A variable centrifugal pump was used to control the flow rate, an impeller mixer to maintain a suspension in the mixing tank (nominal capacity 100 litres, *i.e.* 0.1 m^3) and electromagnetic flow meter to measure the flow rate. Mains water was used as the fluid. The flow loop was filled with suspensions of the four particle species listed in Table 2 at several nominal (weighed) concentrations and run over a range of flow rates. Data from pairs of runs at the two ultrasonic frequencies were generated and combined (in which J_1,

J_2 and M are functions of distance, r, from the transducer), and concentration profiles along a vertical cross-section were constructed using Equation [11]. A nominal value for the speed of sound in water of c = 1480 m s^{-1} and a temperature of T = 20 °C were assumed in all calculations. The experimental apparatus did not include a thermostat and all suspensions were at ambient laboratory temperature. However, regular temperature measurements were taken and a conservative value for the uncertainty in the temperature was estimated to be dT = ±4 °C, and this uncertainty is discussed in more detail in the results section.

The transmitted pulse voltage was 150 V in every run, and each pulse contained two cycles (producing pulse durations of 1 μs for the 2 MHz probe and 0.5 μs for the 4 MHz probe). The position of measurement points was determined by the instrumental software by time gating. Since the speed of sound in the fluid was known, a given time interval between emission of a pulse and receipt of the return signal corresponded to a particular measurement channel/volume. The RMS voltage at each channel was taken over the entire run. For all the runs in the main pipe flow loop, n = 2500 voltage profiles were taken for each run and the system-applied gain and digitisation constant were removed from the raw data in MATLAB in order to generate RMS voltage profiles (V in Equation [2]). A three-sigma noise filter was also applied. The probe oriented at 90° to the mean flow direction receives signals from both scatterers in the flow (*i.e.* suspended particles) and the internal (lower) pipe wall. The latter was used to calibrate the position of that probe. The probe oriented at 135°, however, receives a signal only from suspended sediment, as the component of the emitted pulse that is reflected by the lower pipe wall continues upstream and is backscattered to the probe to a negligible degree.

As can be seen in Figure 1(b), the measurement points for each transducer were not co-located, so it was necessary to perform linear interpolation (of the 2 MHz data). The perpendicular distance, y, from the upper pipe wall was chosen as the common axis. For each run, three physical samples (each of 60 ml) were taken from the mixing tank and a mean value calculated. The sampled concentration or volume fraction is denoted by the subscript s hereafter (*i.e.* M_s and ϕ_s), whereas the nominal (weighed) concentration or volume fraction is denoted by the subscript w (*i.e.* M_w and ϕ_w).

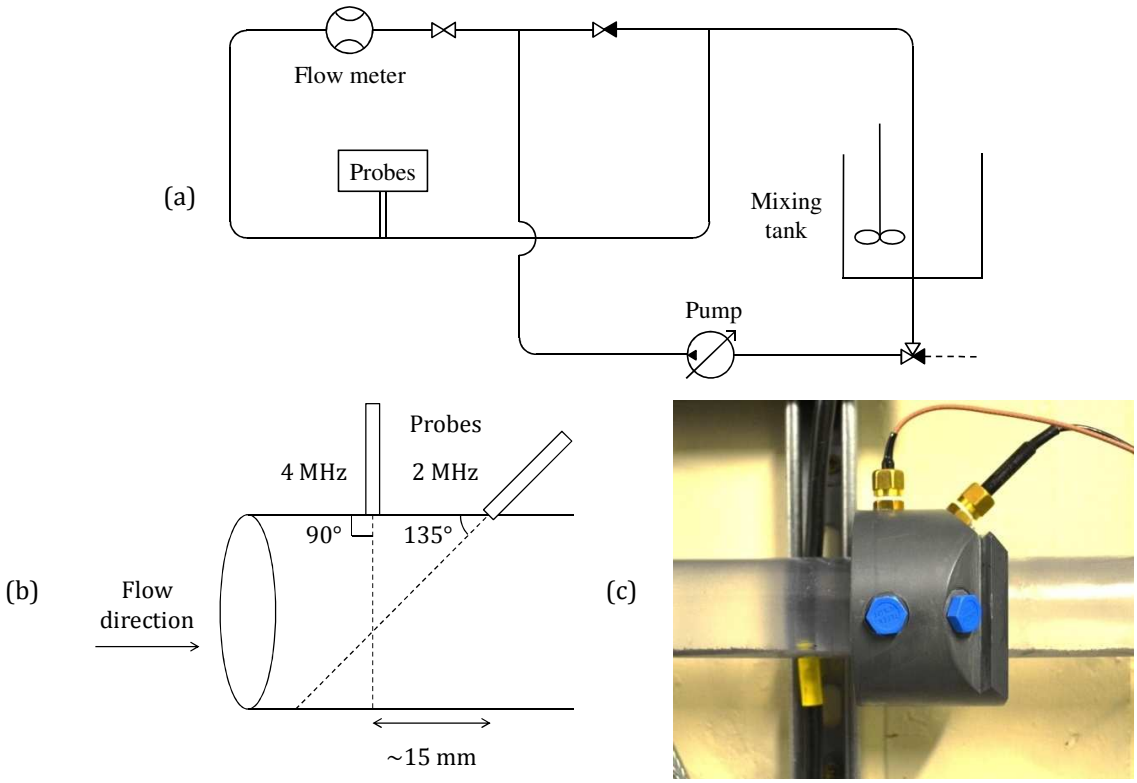

Figure 1: (a) Pipe flow loop schematic, (b) probe mounting geometry schematic and (c) photograph of probes attached to mounting clasp (colour online). Inner diameter, D = 42.6 mm; entry length, L = 3.2 m.

4 Results and discussion

In Section 4.1, the influence of attenuation on computed concentration is explored, and expressions for an acoustic penetration depth, δ_p, and an application-specific limiting particle concentration, M_{lim}, are derived and discussed. In Section 4.2, concentration profiles, computed according to Equation [11] and the method described in Section 2, are presented at two flow rates and three weighed/nominal concentrations for all four particle species. In Section 4.3 and the appendix, the error in M due to uncertainties in the first attenuation coefficient, ξ, is derived explicitly. Then, the error bounds are shown for one run as an example, and the variation in the relative error with distance is shown for the same run, for illustration.

4.1 Acoustic penetration depth and limiting concentration

Although the presence of attenuation by particles in the suspension is required by the model, excessive attenuation will cause the acoustic energy to be extinguished (by scattering and absorption) before it reaches the transducer. The calculations and physical arguments presented in this section are intended as suggestions for scoping future

experiments, as a balance must always be struck between the quality of the received signal and the maximum distance over which data can be gathered.

By inspection of Equations [2], [3] and [8], it is possible to define an acoustic penetration depth, δ_p, over which the acoustic signal will be attenuated by a factor of e^{-1}, such that

$$\delta_p = \frac{1}{2\xi_h M}, \qquad [14]$$

where the factor of two accounts for the fact that the backscattered acoustic signal must traverse the distance to and from the scatterers.

Since ξ_h is known for all particle species (Table 2), it is possible to calculate δ_p for the nominal concentrations used in this study, *i.e.* ϕ_w = 0.5, 1 and 3 % (M_w = 12.4, 24.7 and 72.8 kg m^{-3} for the glass species; M_w = 7.46, 14.9 and 43.7 kg m^{-3} for the two plastic species, respectively). The penetration depths in four representative cases, with the associated flow parameters, are given below, and it should be borne in mind that the diameter of the pipe used in this study is D = 42.6 mm. These examples are intended to illustrate the full range of very slightly attenuating to very strongly attenuating suspensions.

- Case 1: Small glass at f = 2 MHz (ξ_1 = 0.0182) at low concentration (ϕ = 0.5 %, M = 12.8 kg m^{-3}): δ_p = 2.15 m.
- Case 2: Large glass particles at f = 4 MHz (ξ_1 = 0.135) at intermediate concentration (ϕ = 1 %, M = 24.7 kg m^{-3}): δ_p = 15.0 cm.
- Case 3: Small plastic particles at f = 2 MHz (ξ_1 = 0.627) at intermediate concentration (ϕ = 1 %, M = 14.9 kg m^{-3}): δ_p = 5.35 cm.
- Case 4: Large plastic particles at f = 4 MHz (ξ_1 = 2.73) at high concentration (ϕ = 3 %, M = 43.7 kg m^{-3}): δ_p = 4.19 mm.

It is clear from the cases presented above that, for the glass species (Honite 22 and 16), the penetration depth exceeds the required measurement distance (*i.e.* the pipe diameter, D = 42.6 mm), and so it would be expected that data from the entire pipe cross-section could be retrieved. In case 3, however, δ_p is similar in magnitude to D, and so it is reasonable to expect the signal received by the transducer to be significantly, but perhaps not prohibitively, attenuated. In case 4, the penetration depth is less than a quarter of the pipe diameter, and so very little of the emitted acoustic energy would be returned to the transducer. (For example, in case 4, attenuation reduces the emitted signal to 0.004 % of

its strength after travelling a distance of $2D$.)

Alternatively, the influence of attenuation can be assessed from the perspective of the limiting concentration, M_{lim}, which is defined as that at which the desired maximum measurement distance is equal to the penetration depth, such that:

$$M_{lim} = \frac{1}{2\xi\delta_{p,lim}}, \qquad [15]$$

where $\delta_{p,lim}$ is the limiting distance, *i.e.* that corresponding to the limiting concentration. By setting $\delta_{p,lim}$ = D, where D is the pipe diameter, it is possible to find the limiting concentration for the flow conditions described in this study. These values of M_{lim} for each particle type are given in Table 3.

Table 3: Limiting concentration by mass, M_{lim} (kg m^{-3}), calculated *via* Equation [15], for all particle species. Nominal mass concentrations, M_w, corresponding to nominal volume fractions, ϕ_w, used in this study also given, for comparison.

	Small glass (Honite 22)	Large glass (Honite 16)	Small plastic (Guyblast 40/60)	Large plastic (Guyblast 30/40)
M_{lim}				
f = 2 MHz	1,290	1,110	37.4	17.5
f = 4 MHz	338	174	8.57	8.60
M_w				
ϕ_w = 0.5 %	12.4	12.4	7.46	7.46
ϕ_w = 1 %	24.7	24.7	14.9	14.9
ϕ_w = 3 %	72.8	72.8	43.7	43.7

It is clear from Table 3 that the limiting concentration, M_{lim}, is either of a similar magnitude to the nominal concentration, M_w, or exceeds it in several cases. In those cases where $M_{lim} \sim M_w$, the acoustic signal may be attenuated significantly. In those cases where $M_{lim} \ll M_w$, the voltage excited in the transducer may be so low that the particle concentration computed *via* Equation [11] appears to be strongly under-predicted or effectively zero. In these cases, the method is not reliable. It is also important to note that only the attenuation at one frequency needs to be significant (in practice, this will be the higher frequency) for the computed concentration to be affected, since the computation of M depends on both ξ_1 and ξ_2 through Equation [11]. Attenuation will be significant at the lowest nominal concentration (ϕ_w = 0.5 %) for both plastic particle species (Guyblast

40/60 and 30/40), as $M_{lim} \sim M_w$ in that case, and is likely to overwhelm the acoustic signal at the two higher nominal volume fractions (ϕ_w = 1 and 3 %), in which cases $M_{lim} > M_w$. Attenuation may also be significant for the larger glass species (Honite 16) at the highest nominal concentration (ϕ_w = 3 %) if the concentration gradient is such that there is strong segregation towards the lower part of the flow.

The significance of the penetration depths and limiting concentrations are discussed in detail in the next section, in the context of the computed concentration profiles that are presented.

4.2 Computed particle concentration profiles

Concentration profiles computed using Equation [11] and the acoustic coefficients given in Table 2 are presented for all particle species at nominal volume fractions of ϕ_w = 0.5, 1 and 3 % at two Reynolds number, Re ≈ 25 000 and 50 000 (with the exception of the smaller glass species, Honite 22, at the lower flow rate, as the data were not saved correctly during the run).

Profiles for the smaller glass species (Honite 22) at Re ≈ 25 000 and 50 000 are shown in Figure 2 and Figure 3, respectively; for the larger glass (Honite 16) in Figure 4 and Figure 5; for the smaller plastic (Guyblast 40/60) in Figure 6 and Figure 7; and for the larger plastic (Guyblast 30/40) in Figure 8 and Figure 9. The actual Reynolds numbers and the sampled concentrations, M_s, are given in the captions to the figures. It should be noted that the axes are reversed for ease of visualisation. The abscissa (on the vertical axis) is normalised by the pipe diameter, D, to give y'/D, and the ordinate (on the horizontal axis) by the nominal mass concentration, M_w (and the nominal volume fraction, ϕ_w) to give M/M_w (which is identical to ϕ/ϕ_w). It is important to note that only the lower half of the pipe flow is shown in the figures, *i.e.* $-0.5 < y'/D < 0$.

It is important to note that the flow rates used in this study are well above the threshold for incipient particle motion, found to occur at Re ≈ 6 500 (Rice, 2013), for the small plastic particles (Guyblast 40/60) and is likely to be similar (although slightly higher) for the larger plastic species and significantly higher for both glass species (Honite 22 and 16), which, although more dense, are an order of magnitude smaller than the plastic species. Moreover, a novel method for measuring the critical deposition velocity, U_c, and the corresponding Reynolds number, Re_c, which is defined as follows:

$$\mathrm{Re}_c = \frac{U_c D}{\nu}, \qquad [16]$$

was described by Rice *et al.* (2014); the measured values of Re_c for all four particle types are summarised in Table 4, from which it is clear that the results at Re ≈ 25 000 fall below the critical deposition Reynolds number (with the exception of Honite 22 at the lower flow rate: actual Reynolds numbers are Re = 25 900 and 25 600 – as shown in Figure 2 – as compared with Re_c = 19 200, so no moving bed exists in those cases), while the results at Re ≈ 50 000 fall above it. Therefore, the results at Re ≈ 25 000 and 50 000 can broadly be categorised as bed-forming and non-bed-forming, respectively.

Table 4: Critical deposition Reynolds number (Re_c) for all particle species at each nominal volume fraction, ϕ_w. For more details see Rice (2013).

	Small glass (Honite 22)	Large glass (Honite 16)	Small plastic (Guyblast 40/60)	Large plastic (Guyblast 30/40)
ϕ_w = 0.5 %	19 200	26 600	30 600	33 100
ϕ_w = 1 %	25 900	26 900	33 700	37 300
ϕ_w = 3 %	30 100	35 300	39 100	46 900

As noted earlier, there is a surprising scarcity of comparable concentration-profile data at low concentrations in the literature, and many of the data that *are* available are either at too high a concentration (Ekambara *et al.*, 2009; Gillies *et al.*, 2004; Karabelas, 1977; Kaushal and Tomita, 2002b), or were gathered in the presence of a thick bed (Matoušek, 2009; Pugh and Wilson, 1999). The reader is also referred to the studies listed in Table 1.

However, a small number of suitable datasets were found and used for comparison, the flow and particle properties of which are summarised in Table 5, along with details of the corresponding runs generated in this study to which they are compared. Flow properties were quantified by the Reynolds number, Re, and particle properties by the Archimedes number, Ar, a measure of the relative significance of gravitational to viscous forces that is defined as follows:

$$\mathrm{Ar} = \frac{g d^3 (s-1)}{\nu^2}, \qquad [17]$$

where g is the acceleration due to gravity and s is the specific gravity is the particles such that

$$s = \frac{\rho_s}{\rho_w}, \qquad [18]$$

where ρ_w is the density of water.

Table 5: Summary of flow and particle properties, in terms of Re and Ar, for runs where comparison is made to data in literature.			
Case	1	2	3
See figure	Figure 2	Figure 5	Figure 7
Particle type	Small glass	Large glass	Small plastic
This study			
Re	~25 000	~50 000	~50 000
Ar	0.987	6.49	543
ϕ_w (%)	1 and 3	0.5, 1 and 3	0.5, 1 and 3
Reference study			
Reference	Karabelas (1977)	Kaushal *et al.* (2002)	Roco and Balakrishnam (1985); Capecelatro and Desjardins (2013)
Re	32 700	165 000	85 500
Ar	2.08	5.20	72.7
ϕ (%)	0.322	4.09	8.41

4.2.1 Results: glass particle species

In this sub-section, the computed particle concentration profiles with the glass (Honite) species are described specifically. Profiles for the smaller glass particles (Honite 22) at Re ≈ 25 000 and Re ≈ 50 000 are shown in Figure 2 and Figure 3, respectively, and for the larger glass particles (Honite 16) in Figure 4 and Figure 5. The corresponding results for the plastic (Guyblast) species are described in Section 4.2.2.

The first and most striking trend that can be observed is that M generally increased with distance from the pipe centreline: it is clear that heterogeneous suspensions were produced in all cases, as would be expected for a real suspension with gravitational settling. Moreover, the degree of heterogeneity was greater at the lower flow rates (Re ≈ 25 000, *i.e.* settling flows). For example, in the case of the larger glass particles (Honite 16), it can be seen from Figure 4 (Re ≈ 25 000) and Figure 5 (Re ≈ 50 000) that the mass concentration, M, at ϕ_w = 0.5 % (M_w = 12.4 kg m^{-3}) increases to $M/M_w \approx 2.8$ near the pipe bottom at the lower flow rate. In this case, a moving bed is present, as the mean flow velocity is below the critical deposition velocity. At the higher flow rate, however, the

concentration reaches a maximum of $M/M_w \approx 1.2$ in the same region, as no bed is present and the solid fraction is fully suspended: the mean flow velocity is above the critical deposition velocity.

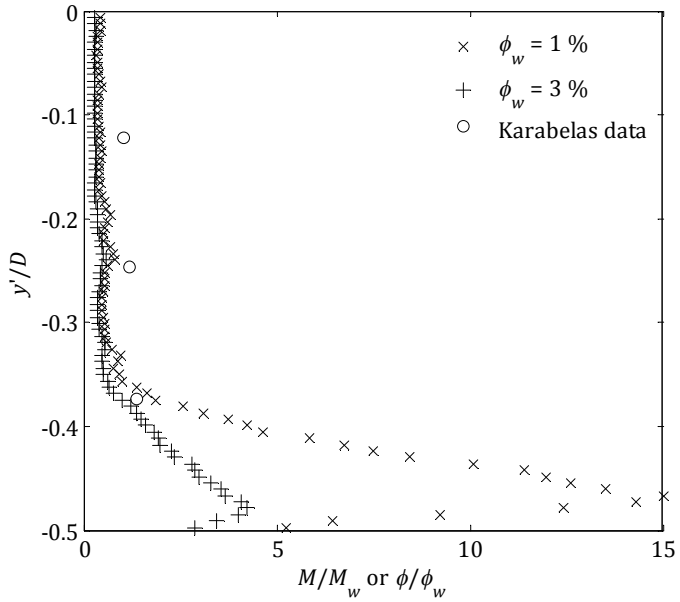

Figure 2: Normalised concentration profiles, M/M_w or ϕ/ϕ_w, *vs*. reduced distance from centreline, y'/D. Small glass spheres (Honite 22, d_{50} = 41 μm) at Re = 25 900 and 25 600; ϕ_w = 1 and 3 %; M_w = 24.7 and 72.8 kg m^{-3} (M_s = 24.3 and 67.0 kg m^{-3}), respectively. Circles from Karabelas (1977), Re = 32 700 (see Table 5). Lower half of flow shown.

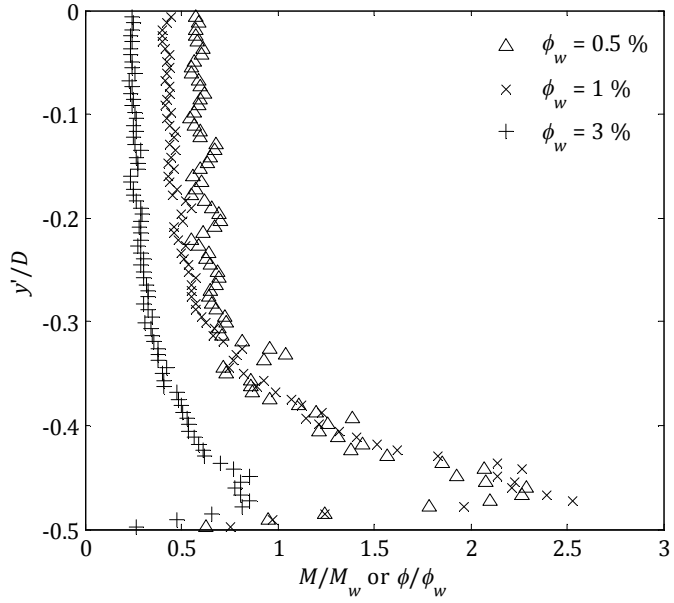

Figure 3: Normalised concentration profiles, M/M_w or ϕ/ϕ_w, *vs*. reduced distance from centreline, y'/D. Small glass spheres (Honite 22, d_{50} = 41.0 μm) at Re = 53 100, 52 700 and 52 100; ϕ_w = 0.5, 1 and 3 %; M_w = 12.4, 24.7 and 72.8 kg m^{-3} (M_s = 13.4, 27.4 and 79.9 kg m^{-3}), respectively. Lower half of flow shown.

The same distinction can be observed in the results for the smaller glass species (Honite 22) in Figure 2 (Re ≈ 25 000) and Figure 3 (Re ≈ 50 000). In the first case, Figure 2, some results from Karabelas (1977), who sampled the concentration physically with a pump, are also included in the plot. Although the number of data from Karabelas are limited (three), it is clear that the inversion method described here under-predicts the particle concentration in the region $-0.3 < y'/D < 0$ (two points) but gives a good prediction in the lowest region (one point). It is not thought that differences in the flow and particle properties are able to explain to the discrepancy. Although the Reynolds number was lower in this study than in the Karabelas (1977) study (Re ≈ 25 000 *vs*. Re = 32 700; see Table 5), which would be expected to produce a more heterogeneous suspension, the Archimedes number was lower, so that the particles would be expected to be more easily suspended at a given flow rate.

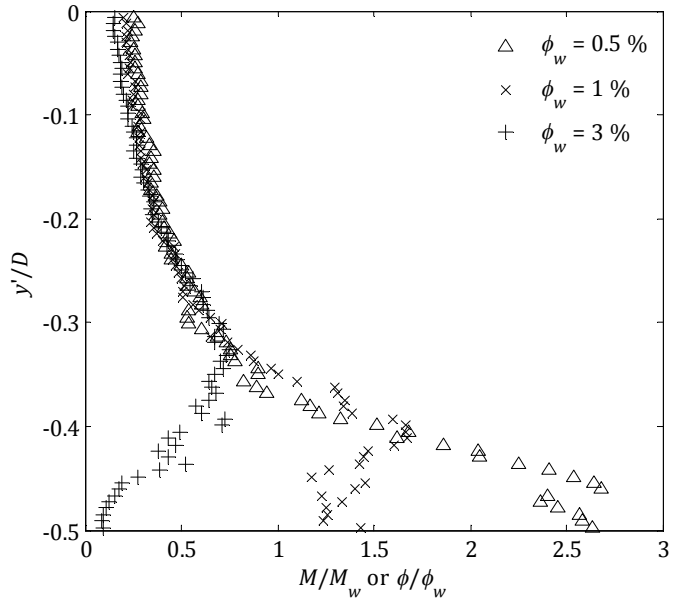

Figure 4: Normalised concentration profiles, M/M_w or ϕ/ϕ_w, *vs*. reduced distance from centreline, y'/D. Large glass spheres (Honite 16, d_{50} = 77.0 μm) at Re = 25 100, 25 400 and 25 000; ϕ_w = 0.5, 1 and 3 %; M_w = 12.4, 24.7 and 72.8 kg m^{-3} (M_s = 7.30, 10.9 and 28.2 kg m^{-3}), respectively. Lower half of flow shown.

The most plausible explanations for the discrepancy are thought to be: (a) that the glass particles used in this study had a relatively wide size distribution, and the increase in concentration towards the bottom of the pipe (and corresponding rarefaction towards the centreline) is a result of larger particles segregating relative to the smaller; and (b) that a certain proportion of particles are known to have settled out in the mixing tank, so the true concentration in the test is likely to have been slightly less than the nominal amount

(as is tentatively confirmed by the sampled concentrations, M_s, given in the caption to Figure 2 and, indeed, the figures for all runs at Re ≈ 25 000).

In addition to evidence of segregation at both flow rates, there was generally also a decrease in ambient concentration, as quantified by the sampled concentration, M_s, relative to the nominal concentration, M_w, with decreasing flow rate, where by "ambient" is meant in the region well above the pipe bottom. This observation is physically realistic, as the lower the flow rate, the larger the proportion of suspended solids would be expected to settle out of suspension, thereby depleting the ambient concentration.

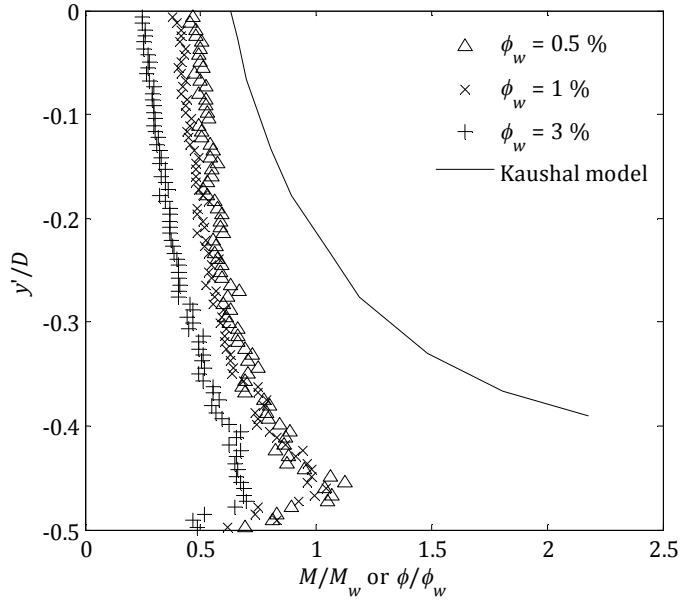

Figure 5: Normalised concentration profiles, M/M_w or ϕ/ϕ_w, *vs*. reduced distance from centreline, y'/D. Large glass spheres (Honite 16, d_{50} = 77.0 μm) at Re = 53 100, 51 600 and 51 100; ϕ_w = 0.5, 1 and 3 %; M_w = 12.4, 24.7 and 72.8 kg m^{-3} (M_s = 13.6, 20.9 and 54.8 kg m^{-3}), respectively. Solid line from Kaushal *et al.* (2002), Re = 165 000 (see Table 5). Lower half of flow shown.

As discussed in more detail in a related paper Rice *et al.* (2014), the propagation of acoustic energy through a suspension depends on both absorption and scattering processes, and when formulated from the frame of reference of a single, monostatic transducer arrangement, these processes manifest themselves as apparent attenuation and backscatter; these are incorporated into the mathematical model used here as ξ and K, respectively, through Equation [2]. It is with these processes in mind that the hump-like structures observed in the majority of the concentration profiles presented here, are discussed. The humps can generally be regarded as an indicator of the point in space at which the backscatter strength of the suspension is overwhelmed by the attenuation, which has a stronger dependence on concentration than does backscatter (Thorne and

Hanes, 2002), through Equation [2].

In a weakly attenuating suspension, the received echo voltage will increase with concentration *via* an increase in unattenuated backscattered energy. In this case, only a reflective surface or interface (such as the upper surface of a settled bed) would produce a hump-like structure. (See, for example, the results for the smaller glass species at ϕ_w = 0.5 % in Figure 4.) However, in the more realistic case of an attenuating, heterogeneous suspension with intermediate nominal particle concentration such that $M_{lim} \sim M_w$ at some point with the measurement domain (or rather, over a significant depth, as the attenuation due to suspended particles, α_s, has an integral dependence on M in the general case, according to Equation [7]), the source of the hump-like structures is more complex and is discussed in more detail from the perspective of the plastic particle species in the next subsection.

Lastly, the comparison with some more data from the literature as shown in Figure 5 (Honite 16 at Re ≈ 50 000) is described, a summary of which is given in Table 5. As with the comparison shown in Figure 2 (Honite 22 at Re ≈ 25 000), the computed particle concentration is under-predicted relative to the data taken from the literature, in this case from Kaushal *et al.* (2002). In contrast to the results shown in Figure 2, however, the particle and flow properties – in terms of Ar and Re – go some way to explaining the discrepancy, since Re is lower and Ar (slightly) higher in this study relative to the Kaushal *et al*. study, suggesting the particles in this study would settle more readily, would suffer from depletion due to settling in the mixing tank, and would form a more heterogeneous concentration profile.

4.2.2 Results: plastic particle species

In this sub-section, the computed particle concentration profiles with the plastic (Guyblast) species are described specifically. Profiles for the smaller plastic particles (Guyblast 40/60) at Re ≈ 25 000 and Re ≈ 50 000 are shown in Figure 6 and Figure 7, respectively, and for the larger glass particles (Guyblast 30/40) in Figure 8 and Figure 9. The corresponding results for the glass (Honite) species are described in Section 4.2.1.

It is clear that the trends observed in the suspensions of glass species are broadly similar for the plastic species, *i.e.*: (a) the computed concentration increases with distance from the centreline; (b) the degree of heterogeneity is greater for the settling runs (*i.e.* in which Re ≈ 25 000) than for the non-settling runs (*i.e.* Re ≈ 50 000); and (c) the normalised

ambient concentration appears to decrease as the nominal concentration increases.

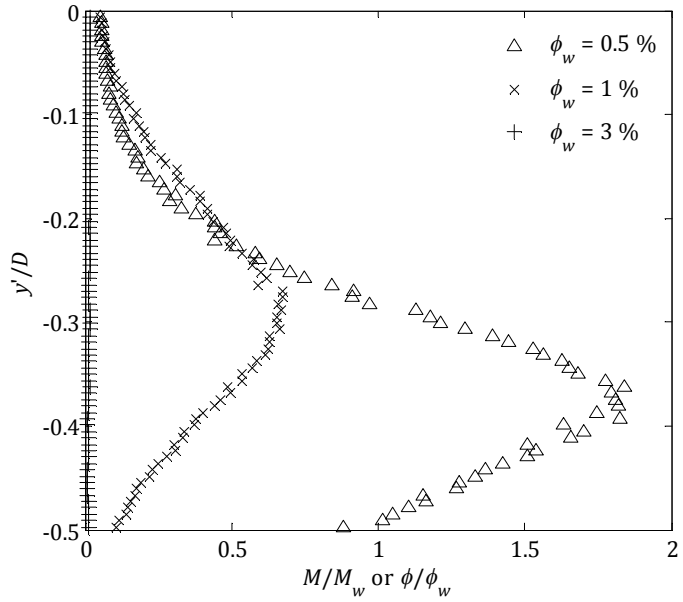

Figure 6: Normalised concentration profiles, M/M_w or ϕ/ϕ_w, *vs*. reduced distance from centreline, y'/D. Small plastic beads (Guyblast 40/60, d_{50} = 468 µm) at Re = 25 600, 25 000 and 24 000; ϕ_w = 0.5, 1 and 3 %; M_w = 7.46, 14.9 and 43.7 kg m^{-3} (M_s = 4.80, 11.3 and 21.4 kg m^{-3}), respectively. Lower half of flow shown.

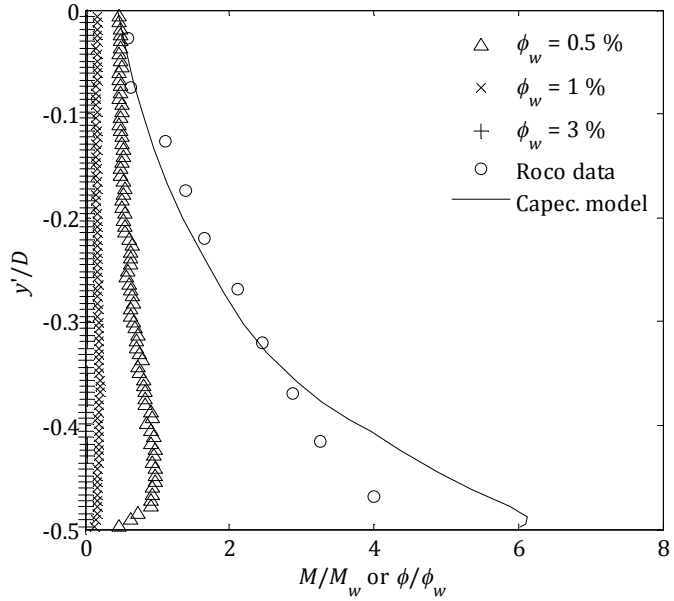

Figure 7: Normalised concentration profiles, M/M_w or ϕ/ϕ_w, *vs*. reduced distance from centreline, y'/D. Small plastic beads (Guyblast 40/60, d_{50} = 468 µm) at Re = 52 300, 51 700 and 51 200; ϕ_w = 0.5, 1 and 3 %; M_w = 7.46, 14.9 and 43.7 kg m^{-3} (M_s = 6.71, 17.3 and 40.5 kg m^{-3}), respectively. Circles and solid line from Roco and Balakrishnam (1985) and Capecelatro and Desjardins (2013), respectively, Re = 85 500 (see Table 5). Lower half of flow shown.

As described in the preceding sub-section, the received echo voltage in a weakly attenuating suspension would be expected to increase proportionally with an increase in particle concentration. However, in the more general case of an attenuating, heterogeneous suspension with intermediate particle concentration (such $M_{lim} \sim M_w$ at some point), the situation is more complex. Good examples of such an intermediate case are the datasets at ϕ_w = 1 and 3 % at the lower flow rate (Re ≈ 25 000) for the larger plastic species (Guyblast 30/40) shown in Figure 8. Both data sets exhibit humps in the region -0.3 $\lesssim y'/D \lesssim$ -0.2. Were these datasets only weakly attenuating, it would be reasonable to assume that the humps correspond to real, physical structures (*i.e.* shear layers), but none were observed visually during the runs, so it must be concluded that the humps correspond, rather, to the regions over which attenuation becomes dominant.

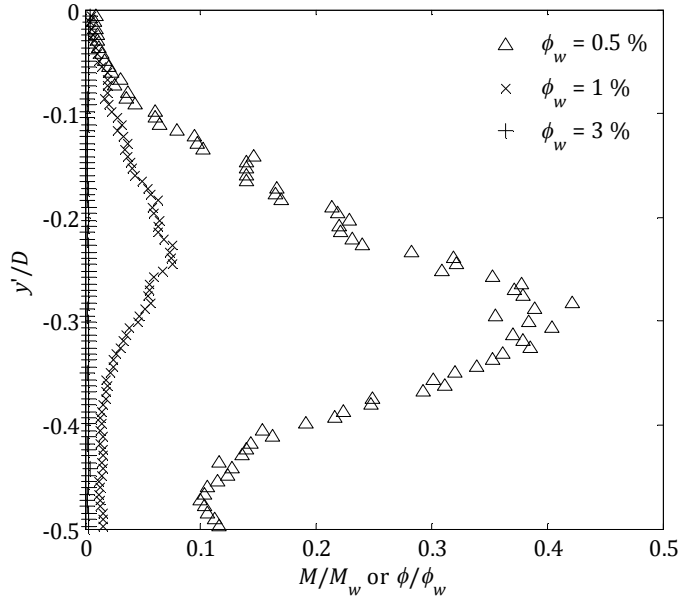

Figure 8: Normalised concentration profiles, M/M_w or ϕ/ϕ_w, *vs*. reduced distance from centreline, y'/D. Large plastic beads (Guyblast 30/40, d_{50} = 691 µm) at Re = 24 300, 24 300 and 23 100; ϕ_w = 0.5, 1 and 3 %; M_w = 7.46, 14.9 and 43.7 kg m^{-3} (M_s = 4.01, 7.56 and 15.7 kg m^{-3}), respectively. Lower half of flow shown.

So, a sensible criterion for an accurate measurement system based on the models and methods presented in this study would be that the point in the measurement domain at which the limiting concentration, M_{lim}, approaches/is exceeded by the actual concentration, M, ought to be within the moving bed/shear layer or, in the case of a stationary bed with a very narrow or non-existent moving component, at the upper surface of the bed. In the latter case, the upper surface may act as a reflective interface so that bed depth measurements can be taken, if the transducer is orientated appropriately. This method was used to determine the bed depth and critical deposition velocity by Rice

(2013), measured values of which were given in Table 4.

Lastly, the comparison in Figure 7 shows results for the small plastic beads at Re ≈ 50 000 and two datasets from the literature - Roco and Balakrishnam (1985) and Capecelatro and Desjardins (2013), both at Re = 85 500 (see Table 5 for more details). Clearly, and as in the other two comparisons with data from the literature (Figure 2 and Figure 5), the concentration is under-predicted in the computed profiles, although less so nearer to the pipe centreline. Several of the explanations invoked in the cases of Figure 2 and Figure 5 are of relevance here – namely the higher Reynolds number and lower Archimedes number (Ar = 72.7) in the reference studies – but the additional issue of strong attenuation must also be noted. The results at ϕ_w = 1 % and 3 % demonstrate that the acoustic signal does not penetrate far into the suspension before being almost entirely attenuated *via* absorption and multiple scattering. Strong attenuation is also evident in the results ϕ_w = 0.5 %, although a hump in M is visible with a peak in the region -0.4 < y'/D < -0.3.

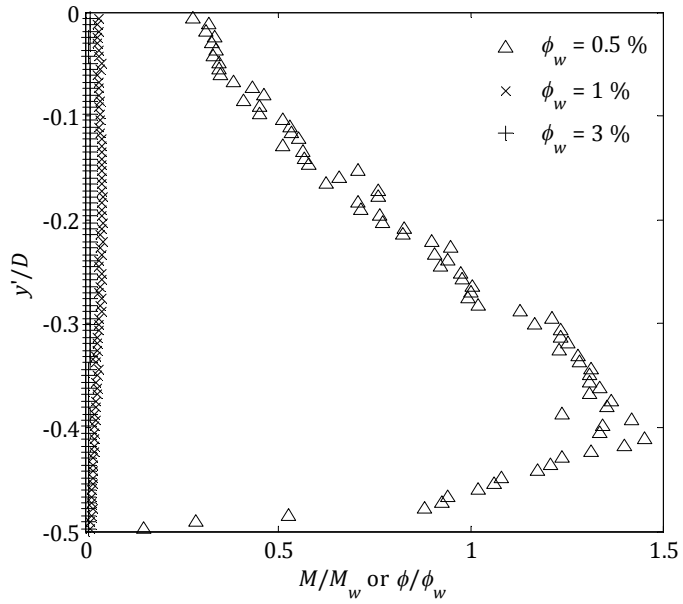

Figure 9: Normalised concentration profiles, M/M_w or ϕ/ϕ_w, *vs*. reduced distance from centreline, y'/D. Large plastic beads (Guyblast 30/40, d_{50} = 691 μm) at Re = 49 700, 50 100 and 48 700; ϕ_w = 0.5, 1 and 3 %; M_w = 7.46, 14.9 and 43.7 kg m^{-3} (M_s = 5.49, 11.2 and 34.3 kg m^{-3}), respectively. Lower half of flow shown.

4.2.3 Discussion

The general trends in the computed particle concentration profiles were described and discussed in Sections 4.2.1 and 4.2.2. Many were common to the glass and plastic particle

species, and all were as expected, notwithstanding the effect of acoustic attenuation, which is below.

It is important to note that the comparisons with data from the literature, as summarised in Table 5, would have shown better agreement if M_s, rather than M_w, had been chosen as the normalising factor in the computed concentration profiles, particularly in the cases where Re ≈ 25 000; in those cases, depletion of the ambient concentration was found to be more significant. However, M_w was chosen for consistency and because M_s was calculated based on relatively small samples (*i.e.* 3 × 60 ml).

Lastly, the influence of attenuation is considered in detail. Even before inspection of the concentration profiles presented in this section, it is to be expected that the larger particle species (*i.e.* Guyblast) would attenuate more strongly than the smaller species (*i.e.* Honite) due to their size. More specifically, expressions for the penetration depth, δ_p, and limiting concentration, M_{lim}, were given and evaluated for the experimental conditions used in this study in Section 4.1. From Table 3, it can be seen that, at f = 4 MHz, M_{lim} = 8.57 and 8.60 kg m^{-3}, respectively, for the two plastic species (Guyblast 40/60 and 30/40), which are similar to the lowest nominal concentration, M_w = 7.46 kg m^{-3} (ϕ_w = 0.5). The acoustic signal would, therefore, be expected to be significantly attenuated. The data for the computed mass concentration, M, in Figure 6 and Figure 7 (smaller plastic species) and in Figure 8 and Figure 9 (larger plastic species) at ϕ_w = 0.5 are, however, reasonable. At ϕ_w = 1 and 3 %, the nominal concentration (M_w = 14.9 and 43.7 kg m^{-3}, respectively) exceeds the limiting concentration at f = 4 MHz for both plastic species (M_{lim} = 8.57 and 8.60 kg m^{-3} for Guyblast 40/60 and 30/40, respectively). It is not surprising, then, that the computed values of M are, as would be expected, very severely underestimated throughout the measurement domain for both plastic species at ϕ_w = 3 % (Figure 6 to Figure 9). Although the attenuation at ϕ_w = 1 % is not quite as severe, it is severe enough to render the results unreliable.

The effect of depletion of ambient concentration due to settling of particles in the mixing tank and, at lower flow rates, in the horizontal parts of the flow loop, was discussed earlier at several points. However, the effect of this depletion on the particle size distribution – and therefore the acoustic properties of the suspensions and computed particle concentrations – was not. Although it is left as a subject for future study, it is suggested that this particle-size depletion could have a significant effect on the computed concentration profiles: particle towards the larger end of the distribution settle more readily, and so any depletion would tend to reduce the actual backscattering and

attenuation coefficients of the suspension relative to the nominal values measured in homogeneous suspensions during the calibration process. However, the intricacies of this effect, and its potential influence on computed concentration profiles *via* J_i and ξ_i, is left as a subject for further study.

To summarise, the differences between the results for the glass and plastic species clearly illustrate the effect of attenuation on real data and, in combination with the expressions for penetration depth and limiting concentration given in Section 4.1, are presented as examples of how acoustically transparent and opaque suspensions can be delineated in real industrial applications.

4.3 Effect of uncertainties in attenuation coefficient, ξ_h

The computed concentration, M, depends on the measured acoustic coefficients, ξ_h and K_h, through Equation [11]. In a related paper (Rice *et al.*, 2014), the influence of uncertainties in K_h on M was derived explicitly and error bounds were presented for some example runs, and a full analysis of experimental errors, including the effect of temperature, pressure, probe mounting angle and beam divergence, was presented by Rice (2013). Here, a complementary error analysis is presented for the influence of ξ_h on M. An expression for the relative error in the mass concentration, $\mathrm{d}M/M$, in terms of the relative error in the attenuation coefficient, $\mathrm{d}\xi_h/\xi_h$, is derived in the appendix and given in Equation [A7].

In order to estimate $\mathrm{d}\xi_h$, the following procedure was followed. By inspection of Equation [10], and defining G'' as follows:

$$G'' = \frac{\partial^2 G}{\partial M \, \partial \mathrm{r}'}, \qquad [19]$$

it can be seen that

$$\frac{\mathrm{d}\xi_h}{\xi_h} = \frac{\mathrm{d}G}{G}. \qquad [20]$$

Example plots of $\partial G/\partial r$ (for the smaller glass species, Honite 22) at both insonication frequencies (f = 2 and 4 MHz) are shown in Figure 10. It is from a linear fit with respect to nominal/weighed concentration, M_w, in such a plot that G'', and therefore ξ_h is calculated in homogeneous suspensions, and the reader is referred to the preceding paper for more

details (Rice *et al.*, 2014). In order to estimate dG and, *via* Equation [20], dξ_h, one datum in each dataset was removed. Specifically, the datum at the highest value of M_w was chosen as this had the greatest effect and was therefore the most conservative choice for estimation of errors.

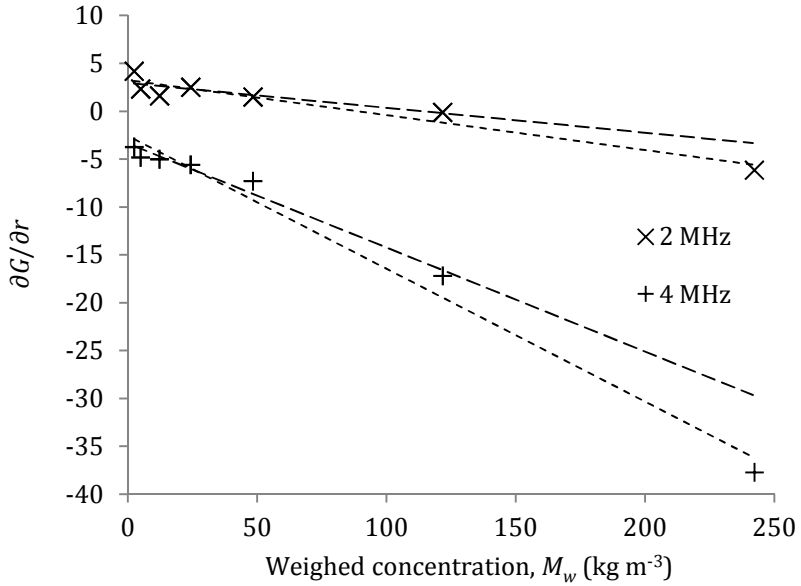

Figure 10: Gradient of G with respect to r *vs.* nominal (weighed) mass concentration, M_w, for Honite 22 glass spheres, for illustration of relative error in measured attenuation coefficient, dξ_h/ξ_h (see text). Fine dashed lines: linear fit to all data. Coarse dashed lines: linear fit to data with highest-M_w datum removed.

The same procedure was repeated for all four particle species, and the relative errors at both frequencies have been compiled in Table 6, from which it can be seen that dξ_h/ξ_h varies between about 3 % for the small glass species at f = 2 MHz and 76 % for the large glass species at f = 2 MHz, with the majority falling in the range of d$\xi_h/\xi_h \approx$ 20-30 %.

Table 6: Relative uncertainties in measured attenuation coefficient, ξ_h.		
Particle type	dξ_{h1}/ξ_{h1} (2 MHz)	dξ_{h2}/ξ_{h2} (4 MHz)
Small glass (Honite 22)	0.287	0.218
Large glass (Honite 16)	0.760	0.192
Small plastic (Guyblast 40/60)	0.0327	0.226
Large plastic (Guyblast 30/40)	0.250	0.0545

The error in the computed mass concentration, M, due to the attenuation coefficient, ξ_{h1}, at 2 MHz for the smaller glass species (Honite 22) at Re = 52 700 and ϕ_w= 1 % was calculated using Equation [3] in the appendix with the value of dξ_{h1}/ξ_{h1} given in Table 6 and is shown

in Figure 11 as an example, with error bounds shown as dashed lines. To aid visualisation, the relative error in the mass concentration, dM/M, is shown explicitly for the same run in Figure 12.

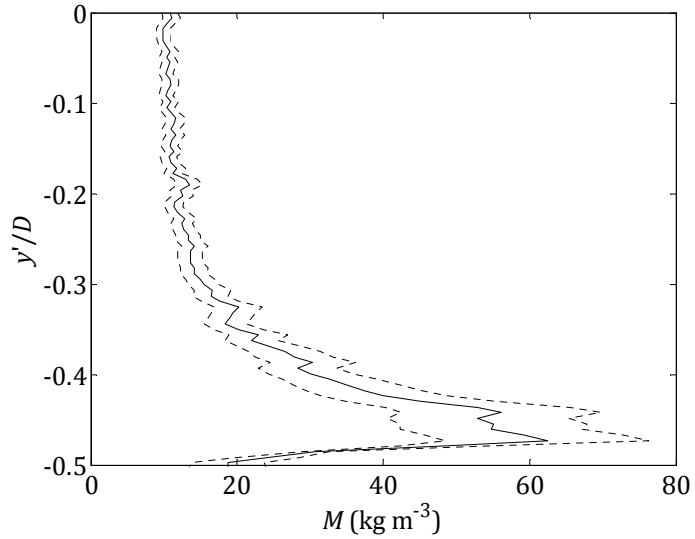

Figure 11: Concentration by mass, M (solid line), *vs*. reduced distance from centreline, y'/D, with error bounds, ±dM, due to attenuation coefficient ξ_1 shown (dashed lines). Small glass spheres (Honite 22, d_{50} = 41 μm) at Re = 52 700 and nominal volume fraction ϕ_w = 1 % (M_s = 27.4 kg m^{-3}). Lower half of flow shown.

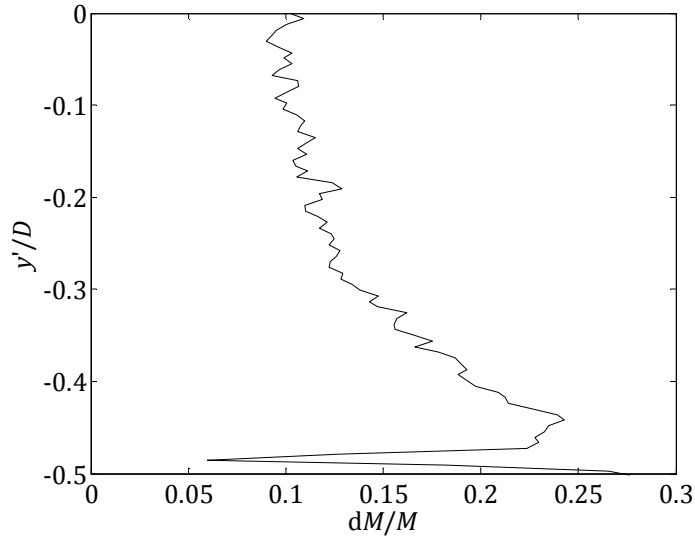

Figure 12: Relative error, dM/M, in calculated mass concentration due to attenuation coefficient ξ_1 *vs.* reduced distance from centreline, y'/D. Small glass spheres (Honite 22, d_{50} = 41 μm) at Re = 52 700 and nominal volume fraction ϕ_w = 1 % (M_s = 27.4 kg m^{-3}). Lower half of flow shown.

It can be seen from both Figure 11 and Figure 12 that both the relative and absolute errors in M generally increase with distance from the upper pipe wall. The magnitude of dM/M

increases with distance from the centreline (reaching a maximum of $\mathrm{d}M/M \approx 25$ % near the pipe bottom) as would be expected from Equation [A7] in general, since the magnitude of the $|\log(J_1/J_2)|$ term will generally increase with distance, as the ratio J_1/J_2 will diverge from unity because the attenuation is stronger at one ultrasonic frequency than the other. This is equally true for the error due to ξ_2, which has an identical algebraic form as Equation [A7].

4.4 Effect of uncertainties in ambient temperature, T

As noted in the methodology, the temperature of the experimental apparatus was not controlled thermostatically. In order to put the influence of the uncertainty in the temperature, T, into context there follows a derivation of the particle concentration below which the error in the acoustic attenuation due to water caused by $\mathrm{d}T$ became equal to the attenuation due to suspended particles.

As described in a preceding paper (Rice *et al.*, 2014), the attenuation due to water at zero salinity depends on insonification frequency and temperature as follows (Ainslie and McColm, 1998):

$$\alpha_w = 0.05641 f^2 \exp\left(-\frac{T}{27}\right), \qquad [21]$$

where α_w is in Np m^{-1}, f is in MHz and T is in °C. The error in α_w can therefore be estimated as follows:

$$\mathrm{d}\alpha_w \approx \mathrm{d}T \left|\frac{\partial \alpha_w}{\partial T}\right|. \qquad [22]$$

Taking the derivative of Equation [21] with respect to temperature gives the following:

$$\frac{\partial \alpha_w}{\partial T} = -2.098 \times 10^{-3} f^2 \exp\left(-\frac{T}{27}\right), \qquad [23]$$

which yields a value of $\partial\alpha_w/\partial T \approx$ -3.98 × 10^{-3} Np m^{-1} K^{-1} for f = 2 MHz at T = 20 °C. The error in the attenuation due to water can be considered to be significant if it is comparable to the attenuation due to suspended particles, *i.e.* if

$$\mathrm{d}\alpha_w \sim \alpha_s. \qquad [24]$$

With Honite 16 at f = 2 MHz (ξ_h = 0.0212: see Table 2) and with dT = 4 °C, if it is assumed that $\alpha_s \approx \xi_h M_w$, then d$\alpha_w$ = ± 0.0160 Np m^{-1}. So, the condition in Equation [24] is satisfied when $M \lesssim 0.75$ kg m^{-3} or $\phi \lesssim 0.03\%$. The error in the attenuation due to water is therefore not likely to have influenced the measured values of ξ_h and K_h because $\phi \approx 0.03\%$ is well below the range of nominal volume fractions used. It should also be noted that the temperature on 10th September 2012 on which the larger glass (Honite 16) calibration runs were performed varied between 20.3 °C (time: 10:30) and 21.4 °C (12:30), so a value of dT = $\pm$ 4 °C is very conservative. For comparison, with Honite 22, the smallest species, insonified at f = 4 MHz, the limiting volume fraction is $\phi \approx 0.04\%$, *i.e.* very similar to that for Honite 16 at f = 2 MHz.

The effect of an uncertainty in the temperature on the acoustic coefficient ξ_h was much less significant for the plastic species, since ξ_h, and therefore the attenuation due to particles at any nominal concentration, is at least an order of magnitude higher. Correspondingly, the limiting concentration below which the uncertainty in the attenuation due to water becomes significant is at least an order of magnitude lower, and the effect can generally be ignored for larger particles (*i.e.* a few hundred microns or more).

To summarise, it was found that the uncertainties in the temperature could affect the total attenuation at lower volume fractions with smaller particles (*i.e.* the Honite species) but not larger particles (*i.e.* Guyblast). These observations demonstrate that the temperature should be controlled, or at least recorded, quite accurately: it is suggested that in future experiments the temperature be measured *in every run* to an accuracy of dT = ± 1 °C or better, and that the exact temperature be accounted for explicitly at the data processing stage. As stated earlier, in the results presented in this study a nominal temperature of T = 20 °C was assumed throughout.

However, it is important to note that the error due to temperature variations is likely to be insignificant compared to the error due to attenuation at higher volume fractions for larger particles, as is clear from Figure 6 and Figure 9 in the previous section, in which the signal is almost completely extinguished in some cases.

5 Conclusions

The method of using measured values of ξ_h and K_h in the dual-frequency inversion

technique was found to be successful, and the resulting concentration profiles followed the expected trends. The effects of segregation and bed formation, for example, were clearly observed in the results. A number of concentration profile datasets from the literature were compared with those generated in this study, and although the flow and particle properties differed significantly in terms of the Reynolds and Archimedes numbers, reasonable agreement was found and a number of possible explanations were given to account for the discrepancies.

Complementary sets of computed concentration profiles below and above the critical deposition velocity were presented in order to investigate whether the acoustic method was able to discriminate between the flow regimes. The study was successful in this regard, at least in the case of the two glass particle species. The computed concentration clearly varies more strongly between the pipe centreline and the pipe bottom in the case of the settling flows (*i.e.* Figures 2 and 4) than in non-settling flows (Figures 3 and 5). However, it was not possible to discriminate in the case of the plastic species as attenuation was generally too high because the particles were very large. In fact, particle species spanning a very large range of mean sizes were chosen in order to investigate and quantify the effect of attenuation. The use of a lower acoustic frequency would eliminate the excessive attenuation and increase the measurable distance: the larger the suspended particles, the lower the frequency must be, in general. However, the lower the frequency that is used, the lower the spatial resolution that can be achieved.

The limitation imposed on the method by acoustic attenuation was investigated in detail, and a delineation between weakly and strongly attenuating suspensions was made quantitatively through the acoustic penetration depth, δ_p, and the limiting concentration, M_{lim}, which was contrived to be application-specific. The expressions for δ_p and M_{lim} given here are presented with the intention that they can be used to select the most suitable acoustic frequencies for a particular set of flow conditions and particle properties. In future studies, it would be advantageous to measure acoustic attenuation with a bi-static system – *i.e.* by transmission – as well as by backscatter. This would provide valuable additional information about the scattering and absorption behaviour of the particle species being tested. In addition, it should be noted that methods exist for calculating suspended particle size as well as concentration (Hurther *et al.*, 2011; Thorne and Buckingham, 2004; Thorne and Hurther, 2014). The potential engineering applications of such inversions are obvious but have not been exploited to a large degree.

It is thought that the novel method used in this study has great potential in a range of

engineering industries where *in-situ* characterisation of flowing or settling suspensions is required, particularly if chemical or radiological hazards make access difficult.

Acknowledgements

The present study is based on part of the Ph.D. thesis of H. P. Rice ("Transport and deposition behaviour of model slurries in closed pipe flow", University of Leeds, 2013). The authors wish to thank the Engineering and Physical Sciences Research Council for their financial support of the work reported in this paper under EPSRC Grant EP/F055412/1, "DIAMOND: Decommissioning, Immobilisation and Management of Nuclear Wastes for Disposal". The authors also thank Peter Dawson, Gareth Keevil and Russell Dixon for their technical assistance, and Olivier Mariette at *Met-Flow*, Switzerland, for his support and advice.

References

ADMIRAAL, D. M. AND GARCÍA, M. H. 2000, Laboratory measurement of suspended sediment concentration using an Acoustic Concentration Profiler (ACP), *Exp. Fluids,* 28**,** 116-127.

AINSLIE, M. A. AND MCCOLM, J. G. 1998, A simplified formula for viscous and chemical absorption in sea water, *J. Acoust. Soc. Am.,* 103**,** 1671-1672.

CAPECELATRO, J. AND DESJARDINS, O. 2013, Eulerian-Lagrangian modeling of turbulent liquid-solid slurries in horizontal pipes, *Int. J. Multiphas. Flow,* 55**,** 64-79.

CHALLIS, R. E., POVEY, M. J. W., MATHER, M. L. AND HOLMES, A. K. 2005, Ultrasound techniques for characterizing colloidal dispersions, *Rep. Prog. Phys.,* 68**,** 1541-1637.

CROWE, C. T. 2006, *Multiphase Flow Handbook,* Boca Raton, CRC Press, Taylor & Francis.

DORON, P. AND BARNEA, D. 1993, A three-layer model for solid-liquid flow in horizontal pipes, *Int. J. Multiphas. Flow,* 19**,** 1029-1043.

DORON, P. AND BARNEA, D. 1995, Pressure drop and limit deposit velocity for solid-liquid flow in pipes, *Chem. Eng. Sci.,* 50**,** 1595-1604.

DORON, P., GRANICA, D. AND BARNEA, D. 1987, Slurry flow in horizontal pipes - experimental and modeling, *Int. J. Multiphas. Flow,* 13**,** 535-547.

DOWNING, A., THORNE, P. D. AND VINCENT, C. E. 1995, Backscattering from a suspension in the near field of a piston transducer, *J. Acoust. Soc. Am.,* 97**,** 1614-1620.

DURAND, R. AND CONDOLIOS, E. 1952. The hydraulic transport of coal and solids materials in pipes. *Colloquium on the Hydraulic Transport of Coal.* National Coal Board, London.

EKAMBARA, K., SANDERS, R. S., NANDAKUMAR, K. AND MASLIYAH, J. H. 2009, Hydrodynamic simulation of horizontal slurry pipeline flow using ANSYS-CFX, *Ind. Eng. Chem. Res.,* 48**,** 8159-8171.

FURLAN, J. M., MUNDLA, V., KADAMBI, J., HOYT, N., VISINTAINER, R. AND ADDIE, G. 2012, Development of A-scan ultrasound technique for measuring local particle concentration in slurry flows, *Powder Technol.,* 215-16**,** 174-184.

GILLIES, R. G., SCHAAN, J., SUMNER, R. J., MCKIBBEN, M. J. AND SHOOK, C. A. 2000, Deposition velocities for Newtonian slurries in turbulent flow, *Can. J. Chem. Eng.,* 78**,** 704-708.

GILLIES, R. G. AND SHOOK, C. A. 1994, Concentration distributions of sand slurries in horizontal pipe flow, *Particul. Sci. Technol.,* 12**,** 45-69.

GILLIES, R. G. AND SHOOK, C. A. 2000, Modelling high concentration settling slurry flows, *Can.*

J. Chem. Eng., 78**,** 709-716.
GILLIES, R. G., SHOOK, C. A. AND WILSON, K. C. 1991, An improved two layer model for horizontal slurry pipeline flow, *Can. J. Chem. Eng.,* 69**,** 173-178.
GILLIES, R. G., SHOOK, C. A. AND XU, J. H. 2004, Modelling heterogeneous slurry flows at high velocities, *Can. J. Chem. Eng.,* 82**,** 1060-1065.
HANES, D. M. 2012, On the possibility of single-frequency acoustic measurement of sand and clay concentrations in uniform suspensions, *Cont. Shelf Res.,* 46**,** 64-82.
HANES, D. M., VINCENT, C. E., HUNTLEY, D. A. AND CLARKE, T. L. 1988, Acoustic measurements of suspended sand concentration in the C^2S^2 experiment at Stanhope Lane, Prince Edward Island, *Mar. Geol.,* 81**,** 185-196.
HARBOTTLE, D., FAIRWEATHER, M. AND BIGGS, S. 2011, The minimum transport velocity of colloidal silica suspensions, *Chem. Eng. Sci.,* 66**,** 2309-2316.
HAY, A. E. 1991, Sound scattering from a particle-laden, turbulent jet, *J. Acoust. Soc. Am.,* 90**,** 2055-2074.
HURTHER, D., THORNE, P. D., BRICAULT, M., LEMMIN, U. AND BARNOUD, J.-M. 2011, A multi-frequency Acoustic Concentration and Velocity Profiler (ACVP) for boundary layer measurements of fine-scale flow and sediment transport processes, *Coast. Eng.,* 58**,** 594-605.
KARABELAS, A. J. 1977, Vertical distribution of dilute suspensions in turbulent pipe flow, *AlChE J.,* 23**,** 426-434.
KAUSHAL, D. R., SATO, K., TOYOTA, T., FUNATSU, K. AND TOMITA, Y. 2005, Effect of particle size distribution on pressure drop and concentration profile in pipeline flow of highly concentrated slurry, *Int. J. Multiphas. Flow,* 31**,** 809-823.
KAUSHAL, D. R. AND TOMITA, Y. 2002a, An improved method for predicting pressure drop along slurry pipeline, *Particul. Sci. Technol.,* 20**,** 305-324.
KAUSHAL, D. R. AND TOMITA, Y. 2002b, Solids concentration profiles and pressure drop in pipeline flow of multisized particulate slurries, *Int. J. Multiphas. Flow,* 28**,** 1697-1717.
KAUSHAL, D. R. AND TOMITA, Y. 2013, Prediction of concentration distribution in pipeline flow of highly concentrated slurry, *Particul. Sci. Technol.,* 31**,** 28-34.
KAUSHAL, D. R., TOMITA, Y. AND DIGHADE, R. R. 2002, Concentration at the pipe bottom at deposition velocity for transportation of commercial slurries through pipeline, *Powder Technol.,* 125**,** 89-101.
LEE, T. H. AND HANES, D. M. 1995, Direct inversion method to measure the concentration profile of suspended particles using backscattered sound, *J. Geophys. Res.-Oceans,* 100**,** 2649-2657.
MATOUŠEK, V. 2009, Concentration profiles and solids transport above stationary deposit in enclosed conduit, *J. Hydraul. Eng.-ASCE,* 135**,** 1101-1106.
MCCLEMENTS, D. J. 1991, Ultrasonic characterization of emulsions and suspensions, *Adv. Colloid Interface Sci.,* 37**,** 33-72.
OROSKAR, A. R. AND TURIAN, R. M. 1980, The critical velocity in pipeline flows of slurries, *AlChE J.,* 26**,** 550-558.
POVEY, M. J. W. 1997, *Ultrasonic Techniques for Fluids Characterization,* San Diego, Academic Press.
PUGH, F. J. AND WILSON, K. C. 1999, Velocity and concentration distributions in sheet flow above plane beds, *J. Hydraul. Eng.-ASCE,* 125**,** 117-125.
RICE, H. P. 2013, *Transport and deposition behaviour of model slurries in closed pipe flow,* Ph.D., University of Leeds.
RICE, H. P., FAIRWEATHER, M., HUNTER, T. N., MAHMOUD, B., BIGGS, S. AND PEAKALL, J. 2014, Measuring particle concentration in multiphase pipe flow using acoustic backscatter: Generalization of the dual-frequency inversion method, *J. Acoust. Soc. Am.,* 136**,** 156-169.
ROCO, M. C. AND BALAKRISHNAM, N. 1985, Multi-dimensional flow analysis of solid-liquid mixtures, *J. Rheol.,* 29**,** 431-456.
ROCO, M. C. AND SHOOK, C. A. 1985, Critical deposit velocity in slurry flow, *AlChE J.,* 31**,** 1401-

1404.
SHOOK, C. A., DANIEL, S. M., SCOTT, J. A. AND HOLGATE, J. P. 1968, Flow of suspensions in pipelines, Part 2: Two mechanisms of particle suspensions, *Can. J. Chem. Eng.,* 46**,** 238-244.
SOEPYAN, F. B., CREMASCHI, S., SARICA, C., SUBRAMANI, H. J. AND KOUBA, G. E. 2014, Solids transport models comparison and fine-tuning for horizontal, low concentration flow in single-phase carrier fluid, *AlChE J.,* 60**,** 76-112.
THORNE, P. D. AND BUCKINGHAM, M. J. 2004, Measurements of scattering by suspensions of irregularly shaped sand particles and comparison with a single parameter modified sphere model, *J. Acoust. Soc. Am.,* 116**,** 2876-2889.
THORNE, P. D. AND HANES, D. M. 2002, A review of acoustic measurement of small-scale sediment processes, *Cont. Shelf Res.,* 22**,** 603-632.
THORNE, P. D. AND HARDCASTLE, P. J. 1997, Acoustic measurements of suspended sediments in turbulent currents and comparison with in-situ samples, *J. Acoust. Soc. Am.,* 101**,** 2603-2614.
THORNE, P. D. AND HURTHER, D. 2014, An overview on the use of backscattered sound for measuring suspended particle size and concentration profiles in non-cohesive inorganic sediment transport studies, *Cont. Shelf Res.,* 73**,** 97-118.
THORNE, P. D., HURTHER, D. AND MOATE, B. D. 2011, Acoustic inversions for measuring boundary layer suspended sediment processes, *J. Acoust. Soc. Am.,* 130**,** 1188-1200.
THORNE, P. D. AND MERAL, R. 2008, Formulations for the scattering properties of suspended sandy sediments for use in the application of acoustics to sediment transport processes, *Cont. Shelf Res.,* 28**,** 309-317.
THOSTESON, E. D. AND HANES, D. M. 1998, A simplified method for determining sediment size and concentration from multiple frequency acoustic backscatter measurements, *J. Acoust. Soc. Am.,* 104**,** 820-830.
TSUJI, Y. AND MORIKAWA, Y. 1982, LDV measurement of an air-solid two-phase flow in a horizontal pipe, *J. Fluid Mech.,* 120**,** 385-409.
WASP, E. J., KENNY, J. P. AND GANDHI, R. L. 1977, *Solid-Liquid Flow Slurry Pipeline Transportation,* Clausthal, Trans-Tech Publications.
ZISSELMAR, R. AND MOLERUS, O. 1979, Investigation of solid-liquid pipe flow with regard to turbulence modulation, *Chem. Eng. J.,* 18**,** 233-239.

Appendix: Errors in M due to the attenuation coefficient, ξ_1

The influence of the uncertainty in one variable, ξ_1, on the calculated suspended particle concentration, M, is derived for the general case as an example. This appendix and the derivation within it should be taken as complementary to that given in a related paper (Rice *et al.*, 2014) in which the influence of another variable, K_1, is derived.

The expression for M (Equation [11]) is rewritten as follows:

$$M = AB, \qquad [A1]$$

where

$$A = J_1^{(1-\xi_1/\xi_2)^{-1}} \qquad [A2]$$

and

$$B = J_2^{(1-\xi_2/\xi_1)^{-1}}. \quad [A3]$$

Only the error due to ξ_1 is considered, and those due to ξ_1, K_1 and K_2 are neglected for brevity. The error, dM, in the mass concentration of particles, M, is:

$$\mathrm{d}M = \mathrm{d}\xi_1 \left|\frac{\partial M}{\partial \xi_1}\right| = \mathrm{d}\xi_1 \left|\frac{\partial A}{\partial \xi_1} B + \frac{\partial B}{\partial \xi_1} A\right|. \quad [A4]$$

It remains to find expressions for the two derivatives on the right-hand side of Equation [A4], which are as follows:

$$\frac{\partial A}{\partial \xi_1} = \frac{\xi_2 \log(J_1) J_1^{(1-\xi_1/\xi_2)^{-1}}}{(\xi_2 - \xi_1)^2} = \frac{\xi_2 \log(J_1) A}{(\xi_2 - \xi_1)^2} \quad [A5]$$

and, analogously:

$$\frac{\partial B}{\partial \xi_1} = -\frac{\xi_2 \log(J_2) B}{(\xi_1 - \xi_2)^2}. \quad [A6]$$

Substituting into Equation [A4], noting that ξ is always real and positive, and simplifying, the following expression for the relative error in M due to ξ_1 (and in terms of the relative uncertainty in ξ_1) is obtained:

$$\frac{\mathrm{d}M}{M} = \frac{\mathrm{d}\xi_1}{\xi_1} \frac{\xi_1 \xi_2}{(\xi_2 - \xi_1)^2} \left|\log\left(\frac{J_1}{J_2}\right)\right|. \quad [A7]$$

The error due to ξ_2 takes an analogous form, but is not given here, for brevity.